Numerical simulation of viscous flow past two circular cylinders of different diameters

Ming Zhao [a], Liang Cheng [b,*], Bin Teng [a], Dongfang Liang [b]

[a] *State Key Laboratory of Coastal and Offshore Engineering, Dalian University of Technology, Dalian 116024, China*
[b] *School of Civil and Resource Engineering, University of Western Australia, 35 Stirling Highway, Crawley, WA 6009, Australia*

Abstract

Viscous flow past two circular cylinders of different diameters is simulated by using a finite element method. The diameter ratio between the small cylinder and the large one is 0.25. The Reynolds number based on the diameter of the cylinders is 500 for the large cylinder and 125 for the small cylinder. The gap between the small cylinder and the large cylinder ranges from 0.05 to 1.0 times the diameter of the large cylinder. The position angle of the small cylinder relative to the flow direction ranges from 0 to π. The effects of the gap ratio between the two cylinders and the position angle of the small cylinder on drag and lift coefficients, pressure distributions around the cylinders, the vortex shedding frequencies from the two cylinders and flow characteristics are investigated. The magnitudes and frequencies of the fluctuating forces acting on the two cylinders are compared with those on a single cylinder of an equivalent diameter.
© 2005 Elsevier Ltd. All rights reserved.

Keywords: Two circular cylinders; Vortex shedding; Shedding frequency; Drag and lift

1. Introduction

Flow around two circular cylinders of different diameters is relevant to flow around two pipelines in offshore oil and gas engineering. Due to certain technical requirements and economical considerations, a piggyback pipeline is sometimes laid together with the main pipeline. The piggyback pipeline could be a control umbilical used to control subsea wells from the platform. It is often of a different diameter from the main pipeline. Laying the two pipelines together reduces installation costs. Strapping at a certain intervals along the pipeline is preferable for lay and enables the lines to be stabilized as a single line on the seabed. It is expected that the existence of the piggyback pipeline will have some influences on the hydrodynamic forces on the main pipeline and thus, the way to design the pipeline with a piggyback line. Due to the lack of knowledge on such effects in the offshore oil and gas industry, the current design practice of pipelines simplifies the two pipelines as a single pipe of an equivalent diameter (equals to the sum of the two diameters

and the gap between the two cylinders). The validity of the equivalent diameter design concept has not been well investigated.

Flow past two cylinders, in a tandem or a side-by-side arrangement represents an important and remarkably complex flow configuration. A variety of flow patterns, characterized by the behavior of the wake region, may be discerned as the arrangement of the two circular cylinders is changed. Zdravkovich [1,2] showed that when more than one body was placed in a fluid flow, the resulting forces and vortex shedding pattern were completely different from those on a single body at the same Reynolds number. Most of the recent studies on this topic were concerned with flow past two cylinders of identical diameters. The results with a side-by-side configuration of two cylinders of the same diameter by Bearman and Wadcock [3], Williamson [4] and Kim and Durbin [5] showed that only one wake was formed when the distance between the centers of cylinders (L) is below about 2.2 times of the cylinder diameter (D). Meneghini et al. [6] studied the flow past two circular cylinders of the same diameter in tandem and side-by-side arrangements for Reynolds number Re=200. For the tandem arrangement, they observed a negative drag on the downstream cylinder and that the vortices were shed only from the downstream cylinder if the gap between the centers of the two cylinders is less than 3D. A repulsive force between the two cylinders

* Corresponding author. Tel.: +61 8 6488 3076; fax: +61 8 6488 1018.
E-mail address: cheng@civil.uwa.edu.au (L. Cheng).

was observed by Meneghini et al. [6] when the gap is less than 2*D* for the side-by-side arrangement. Mittal et al. [7] studied the case of two cylinders in tandem and staggered arrangements. The main result observed in the study of Mittal et al. [7] was that the drag on the downstream cylinder increases when it is placed at a staggered arrangement.

Fluid forces on a large circular cylinder can be reduced by a proper placement of a relatively small circular cylinder near the large cylinder. Strykowski and Sreenivasan [8] investigated the suppression of the vortex shedding from a circular cylinder by introducing a small circular cylinder at low Reynolds numbers. Sakamoto et al. [9] and Sakamoto and Haniu [10] studied the suppression of the fluid force acting on a square cylinder and a circular cylinder, respectively, at high Reynolds number in subcritical regime. Dalton et al. [11] also simulated the suppression of lift force on a circular cylinder by a small cylinder numerically. The above researchers classified the method for suppressing fluid forces into two categories: one is due to the control of the boundary layer and the other is due to the control of the shear layers separated from the cylinder surface.

In this study, flow past two circular cylinders of different diameters is investigated numerically. It should be noted that the small cylinder discussed in this study represent a practical pipeline rather than a fluid flow control device. The aim of this study is to investigate the effects of the arrangement of the two cylinders on the vortex shedding flow behind the two-cylinder system. The Navier-Stokes equations are solved using a finite element method. The diameter ratio between the small cylinder and the large cylinder is 0.25. The Reynolds number based on the diameter of the cylinders is 500 for the large cylinder and 125 for the small cylinder. The gap between the small cylinder and the large cylinder ranges from 0.05 to 1.0 times the diameter of the large cylinder. The position angle of the small cylinder relative to the flow direction ranges from 0 to π. The effects of the gap ratio between the two cylinders and the position angle of the small cylinder on drag and lift coefficients, pressure distributions around the cylinders, the vortex shedding frequencies from the two cylinders and flow characteristics are investigated. The magnitudes and frequencies of the forces acting on the two cylinders are compared with those on a single cylinder of the equivalent diameter.

It is understood that the flow investigated in this study is three-dimensional since the Reynolds number base on the large cylinder is greater than the critical Reynolds number of 200 [12,13]. However, the two-dimensional simulations carried out in the present study suit the major purposes of the study. The major aims of this study are to quantify the effects of the piggyback pipeline on the main pipeline and validate the equivalent diameter approach. Since, most of the numerical results on the large cylinder and the two-cylinder system are compared with their single cylinder counterparts, it is expected the three-dimensional effects will be largely canceled out in the comparison process. The flow is considered to be perpendicular to the axes of the cylinders.

It is recognized that the Reynolds number investigated in the present study is relatively small in comparison with typical values of the Reynolds number for prototype pipelines. This is based on following considerations. First of all, small values of Reynolds number allow a direct solution of the Navier-Stokes equations being carried out with affordable computational costs. The advantage of the direct solution of the Navier-Stokes equations is that numerical results are not contaminated by potential errors introduced by a turbulence model. The use of a fine computational mesh will substantially reduce the errors introduced by inadequate grid resolution in the direct solution of the Navier-Stokes equations, especially for cases of small Reynolds number flows. Secondly, the inherent three-dimensionality for this particular flow is relatively weak at small values of Reynolds number. Finally, it is well understood that the vortex shedding characteristics from a circular cylinder are less dependent on Reynolds number within the subcritical Reynolds number regime. The Reynolds number investigated in the present study is within the subcritical regime. In addition, it is expected that the trends of the effects of the small cylinder on the flow around the large cylinder are independent on the values of Reynolds number in the subcritical regime.

2. Governing equations and numerical method

The two cylinders considered in this study are shown in Fig. 1. The small cylinder represents the piggyback pipeline and the large cylinder represents the main pipeline. The position of the small cylinder can be uniquely determined by the gap between the two cylinders, the diameters of the cylinders and the angle α as shown in Fig. 1. The flow is in the positive direction of the *x*-axis. θ is an angle in the counterclockwise direction, starting from the positive direction of the *x*-axis, as shown in Fig. 1.

The two-dimensional Navier-Stokes equations together with the continuity equation are solved using a three-step finite element method. The three-step finite element method employed in this study shares enough similarities with the method by Jiang and Kawahara [14] and will not be detailed here. It has been demonstrated elsewhere [14] that the temporal integration used in the present study is of third-order accuracy.
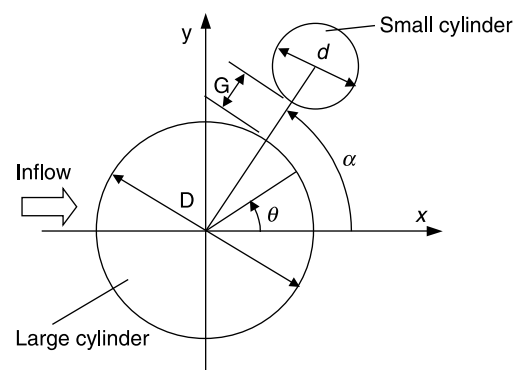
Fig. 1. Definition figure.

The drag and lift force per unit length on the cylinder are calculated as

$$F_d = \int_0^{2\pi} (-p \cos\theta - 2\nu\omega \sin\theta)R d\theta \tag{1}$$

$$F_l = \int_0^{2\pi} (-p \sin\theta d\theta + 2\nu\omega \cos\theta)R d\theta \tag{2}$$

where F_d and F_l are the total drag and lift forces, respectively, R ($=D/2$) is the cylinder radius, ω is the vorticity defined as $\omega = (\partial v/\partial x - \partial u/\partial y)/2$ and θ is the position angle measured from the positive direction of the horizontal axis of the cylinder and positive anticlockwise as shown in Fig. 1. The first term at the right hand side of either Eq. (1) or Eq. (2) represents the contribution of the pressure, while the second term represents the contribution of the shear stress. The drag and lift are then normalized by $\rho U^2/2$ to get the drag and lift coefficients C_d and C_l as

$$C_d = \frac{F_d}{\rho U^2 D/2}, \qquad C_l = \frac{F_l}{\rho U^2 D/2} \tag{3}$$

where U is the free-stream velocity, D is a characteristic dimension of the cylinder.

3. Validation of the numerical model

To validate the numerical model, uniform flow past a singular cylinder for the Reynolds number ranging from 10 to 1000 is simulated. A rectangular flow field of $28D \times 16D$ is divided into 24,458 unstructured finite elements. The total nodal point number is 13,609. The cylinder is located at the mid-height of the computational domain and the distance between the cylinder center and the inlet is $8D$. A typical computational mesh is shown in Fig. 2 and the local mesh near the cylinder surface is shown in Fig. 3. A total of 160 nodal points are placed on the circumference of the cylinder. The structured four-node quadrilateral elements are used near the cylinder surface. In the rest of the calculation domain, three-node triangular elements are used. The minimum mesh size in the radial direction near the cylinder is about $0.01D$. The non-dimensional time step of 0.0025 is used in all the computations.
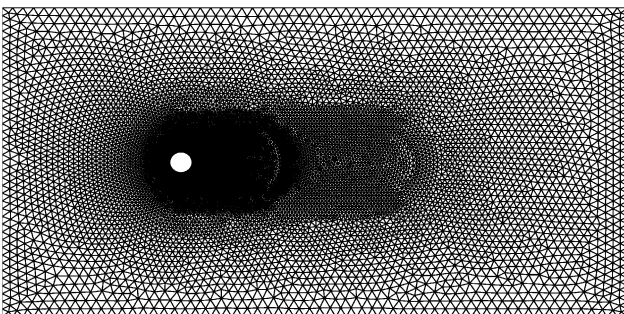
Fig. 2. Computational mesh for flow past a single cylinder.
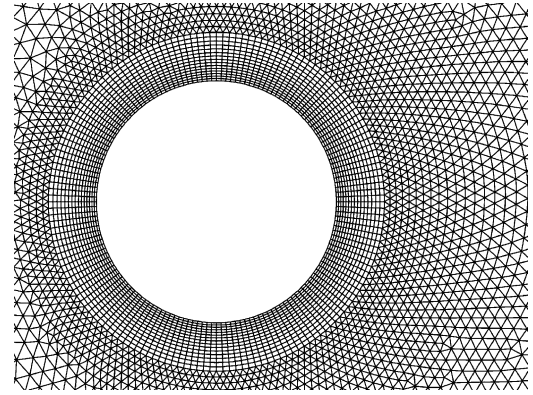
Fig. 3. Detail computational mesh near the cylinder.

At the inflow boundary, the velocity components are specified and pressure is determined from the momentum equations. Symmetric boundary conditions are prescribed on the two lateral boundaries. On the non-slip cylinder surface, zero velocity components are specified and the pressure is obtained by applying the momentum equations in the direction normal to the boundaries. On the outflow boundary, zero normal derivatives of the velocity components and pressure are specified [15,16]. To promote the onset of vortex shedding, an artificial perturbation, corresponding to a clockwise rotation of the cylinder followed by a counter-clockwise rotation, is introduced for a short time at the early stage of the simulation [17].

Fig. 4 shows the time history of the computed drag and lift coefficients for Re$=200$. The vortex shedding can be observed from the time history of the fluctuating force coefficients. Meneghini et al. [6] summarized the results of the Strouhal number for Re$=200$ from different numerical model and experiments. The Strouhal number predicted by the present model for Re$=200$ is 0.196, which is identical to the numerical result by Meneghini et al. [6]. In Fig. 5, the computed time-averaged drag coefficients for Reynolds number from 10 to 100 are compared with the experimental data by Tritton [18] and the finite difference results by Lei et al. [19]. The difference between the two numerical results in Fig. 5 is small, and both sets of the numerical results agree well with the experimental
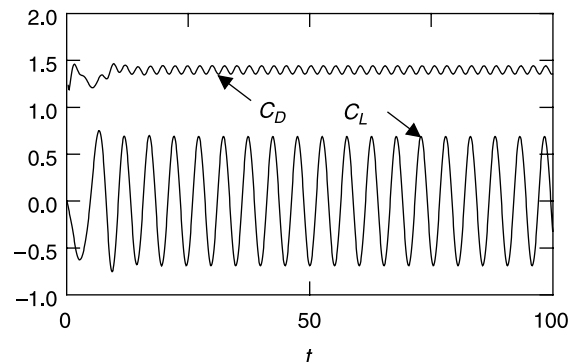
Fig. 4. Time history of the force coefficients for Re$=200$ (singular cylinder).
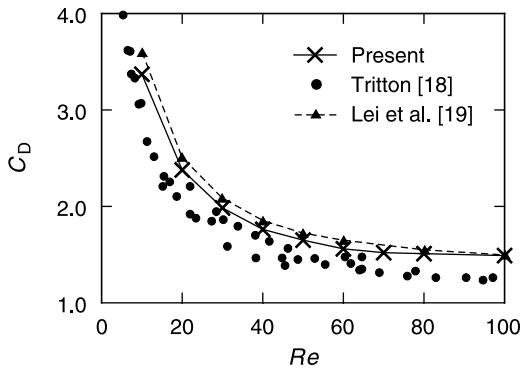
Fig. 5. Comparison of the mean drag coefficient.

Fig. 7. The finite elements near the two cylinders for $G/D=0.1$ and $\alpha=\pi/4$.

data. Fig. 6 shows the comparison of the Strhoual number variations with the Reynolds number for Re < 1000. The two solid lines in the same figure are the envelope lines for the experimental data measured by Roshko [20] (reproduced from Ref. [17]). The Strouhal number is defined in terms of the cylinder diameter (D), the free-stream velocity (U), and the frequency (f) of the oscillation of the lift coefficient as

$$S_t = fD/U \qquad (4)$$

It is seen that the present results and the results by Lei et al. [19] agree well with the experimental data for Reynolds number Re < 200. For Reynolds number Re > 200, the Strouhal numbers predicted in this study and those by Lei et al. [19] are slightly higher than the experimental data. This was demonstrated to be due to the three-dimensional effect for this particular flow since both the present study and the study by Lei et al. are two-dimensional simulations [19].

4. Flow past two circular cylinders of different diameters

The numerical model is then applied to study the flow past two circular cylinders as shown in Fig. 1. The effects of the gap between the two cylinders and the angular position of the small cylinder on the vortex shedding are studied. The ratio of the small cylinder diameter (d) to the large cylinder diameter (D) is $d/D=0.25$. The Reynolds numbers based on the large cylinder and that on the small cylinder are 500 and 125, respectively.

Simulations are carried out for the gap ratio G/D ranging from 0.05 to 1.0 and the position angle α ranging from 0 to π. In all computations, a rectangular computational domain is used. The large cylinder is located at $8D$ from the inflow boundary. The distance between the large cylinder and the outgoing boundary is $20D$. The two lateral boundaries are located at $8D$ away from the large cylinder.

Fig. 7 shows a typical finite element mesh near the cylinders for $G/D=0.1$ and $\alpha=\pi/4$. The structured four-node quadrilateral elements are employed near the surfaces of both cylinders. The rest of the computation domain is discretized using three-node triangular elements. The surfaces of the large and small cylinders are discretized using 160 and 80 nodal points, respectively. The total nodal point number is 14,104 and the total element number is 26,490 for the case of $G/D=0.1$ and $\alpha=\pi/4$. In the other cases, the nodal point number is around 14,000 to 16,000. The mesh characteristics near the cylinders for other cases investigated in this study are very similar to the case shown in Fig. 7. In all calculations, the non-dimensional computational time (Ut/D) step is set to 0.0025. The simulations are carried out up to the non-dimensional time of $Ut/D=200$. In all of the cases studied, regular vortex shedding is observed for $Ut/D>50$. The analyses carried out hereafter are based on the results for $Ut/D>50$.

4.1. Force coefficients

4.1.1. Force coefficients on the large cylinder
Fig. 8 shows the time-averaged drag and lift coefficients on the large cylinder. For the purpose of comparison, the force coefficients on a single cylinder ($G/D=\infty$) are also plotted in Fig. 8. It can be seen from Fig. 8 that the effect of the small cylinder on the mean force coefficients is more significant for the smaller gap ratios ($G/D=0.05$ and 0.1) and near side-by-side locations of the small cylinder (around $\alpha=0.5\pi$). Specifically, the mean drag on the large cylinder is increased significantly for the smaller gap ratios ($G/D=0.05$ and 0.1) and the near side-by-side locations of the small cylinder (around $\alpha=0.5\pi$) (Fig. 8(a)). The maximum increase in the mean drag coefficient on the large cylinder is about 65% at $G/D=0.05$ and $\alpha=0.5\pi$. The level of the mean drag decreases at around

Fig. 6. Comparison of the Strouhal number.
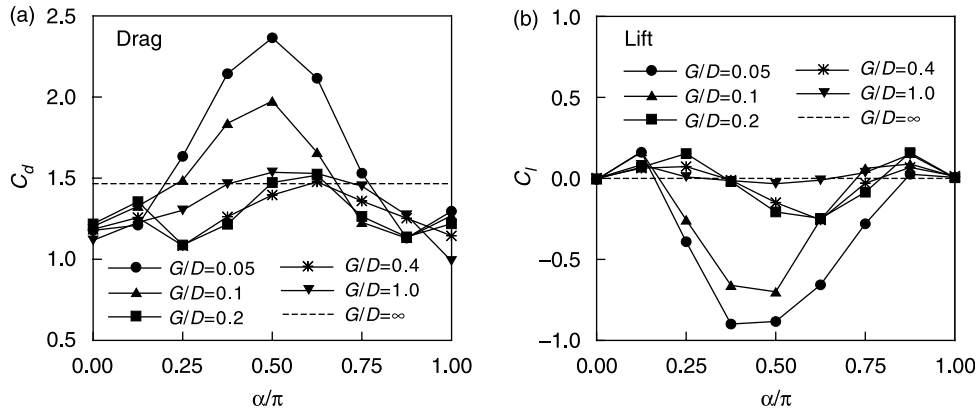
Fig. 8. Time averaged force coefficients on the large cylinder.

$\alpha=0.5\pi$ as the gap ratio G/D increases. It is interesting to observe that the mean drag coefficient on the large cylinder is generally smaller than its single cylinder counterpart ($G/D=\infty$) for the larger gap ratios ($G/D=0.2$, 0.4 and 1.0) except for the case of α around 0.5π. In addition, the mean drag coefficient on the large cylinder decreases when the small cylinder is either behind ($0<\alpha<0.25\pi$) or in front of ($0.75\pi<\alpha<\pi$) the large cylinder regardless of the gap ratio (G/D). Sakamoto et al. [9] found that the reduction of the mean drag on the large cylinder as the small cylinder is located in the front edge of the large cylinder is caused by the displacement of the separation point along the upper surface of the large cylinder. This is also a part of the reasons for considerable drag reduction observed in the present study. It can be seen from Fig. 11(a) that the separation points on both top and bottom sides of the large cylinder moved further downstream for the case of $\alpha=0$. Sakamoto et al. [9] also found that the reduction of the mean drag on the large cylinder as the small cylinder is located at the rear edge of the large cylinder is due to the interference of the small cylinder to the interactions of the shear layers from the top and bottom edges of the large cylinder. It can be seen from Fig. 11(a) that the effect of the small cylinder interference is to increase the base pressure on the large cylinder. The observed effects of the small cylinder on the mean drag coefficient of the large cylinder may be better explained by

examining the pressure distribution around the large cylinder in details. This will be carried out in Section 4.2.

The effects of the small cylinder on the mean lift coefficient of the large cylinder are more or the less similar to those observed for the mean drag coefficient (Fig. 8(b)). In general, the existence of the small cylinder causes a negative mean lift when the small cylinder is located near the top side of the large cylinder (around $\alpha=0.5\pi$). The mean lift can be positive when the small cylinder is located near either the upstream or downstream parts of the large cylinder, depending on the gap ratio between the large cylinder and the small cylinder. The mean lift is zero when the small cylinder is placed either directly in front of ($\alpha=\pi$) or directly behind ($\alpha=0$?) the large cylinder, as expected. The effect of the small cylinder is more significant for smaller gap ratios as in the case for the mean drag.

4.1.2. Force coefficients on the small cylinder

Fig. 9 shows the mean drag and lift coefficients on the small cylinder. It can be seen from Fig. 9(a) that the mean drag on the small cylinder is relatively independent of the range of the gap ratios examined. However, the mean drag on the small cylinder is indeed affected by the angular location of the small cylinder. The mean drag coefficient is larger than its single cylinder counterpart ($G/D=\infty$) when the small cylinder is
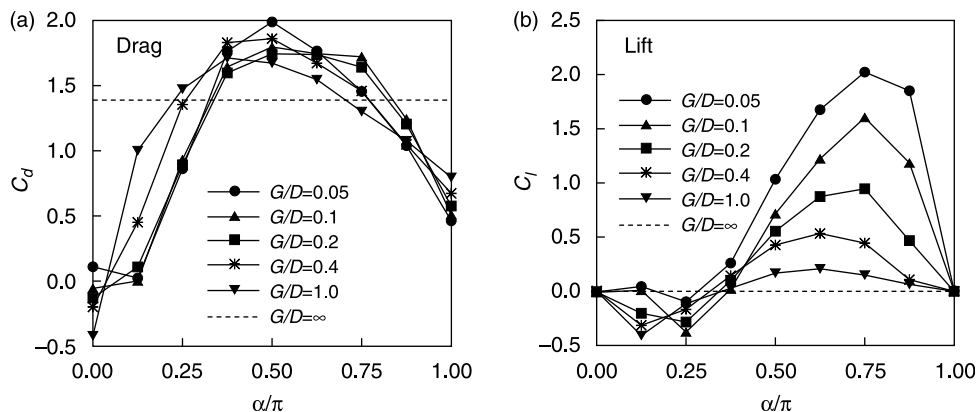
Fig. 9. Time averaged force coefficients on the small cylinder.
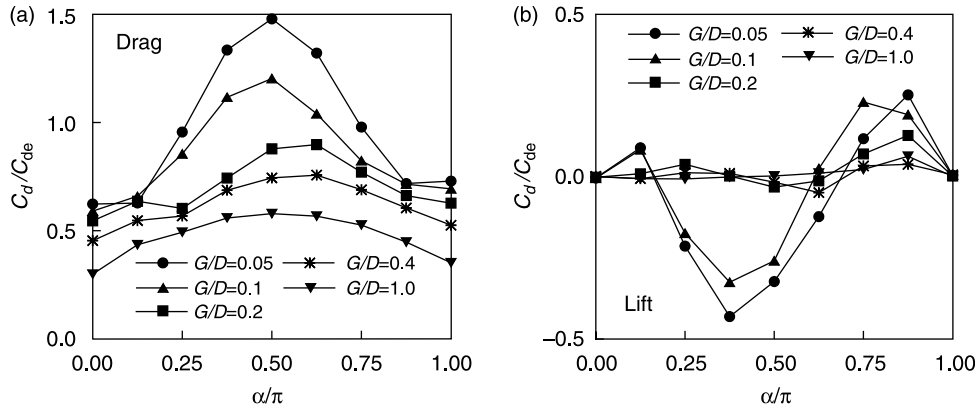
Fig. 10. Normalized total mean force coefficients on the two-cylinder system.

located at around the top side of the large cylinder ($0.3\pi < \alpha < 0.75\pi$). The mean drag coefficient on the small cylinder is smaller than its single cylinder counterpart when the small cylinder is placed outside this area. The mean drag coefficient on the small cylinder decreases as it is moved into the wake of the large cylinder.

It can be seen from Fig. 9(b) that the mean lift on the small cylinder is dependent on both the gap ratio and the angular location of the small cylinder when the small cylinder is away from the wake region of the large cylinder ($\alpha > 0.3\pi$). It can be observed from Fig. 9(b) that the smaller the gap, the larger the mean lift coefficient increases. The mean lift on the small cylinder is positive upward when the small cylinder is outside of the wake region of the large cylinder. The maximum mean lift takes places at $\alpha = 0.75\pi$ and $G/D = 0.05$.

4.1.3. Total force coefficients on the two-cylinder system

Total forces acting on the two-cylinder system are of great importance to pipeline designs. Due to the lack of knowledge on this topic, the current design practice of pipelines simplifies the two cylinders as a single pipe of an equivalent diameter ($D_e = D + d + G$) and then uses the force coefficients derived for a single pipeline to calculate total forces. There are

concerns that such a design concept may not be representative of the real situation.

To examine the validity of the equivalent diameter concept in terms of hydrodynamic forces, the total mean force coefficients (based on the equivalent diameter) acting on the two cylinders are normalized using the corresponding mean drag coefficient acting on a cylinder of an equivalent diameter and are plotted in Fig. 10. C_{de} is the mean drag coefficient on a single cylinder of the equivalent diameter in Fig. 10. It can be seen from Fig. 10(a) that the total mean drag coefficient on the cylinders is generally smaller than its counterpart on an equivalent cylinder for most of the gap ratios and angular locations of the small cylinder except for very small gap ratios, i.e. $G/D = 0.05$ and $G/D = 0.1$, where total mean drag coefficient is greater than that on the equivalent cylinder for roughly $0.25\pi < \alpha < 0.75\pi$. It seems to be true that the smaller the gap ratio, the larger total mean drag coefficient on the two cylinders is. At the minimum gap ratio examined ($G/D = 0.05$), the total mean drag coefficient could be 1.5 times as large as that on the equivalent cylinder when $\alpha = 0.5\pi$. For $\alpha = 0.5\pi$, the total mean lift force coefficient on the two cylinders is non-zero for smaller gap ratios $G/D = 0.05$ and 0.1. The mean lift could be downward or upward depending on the location of the small cylinder. For $G/D = 0.2$, 0.4 and 1.0, the total mean
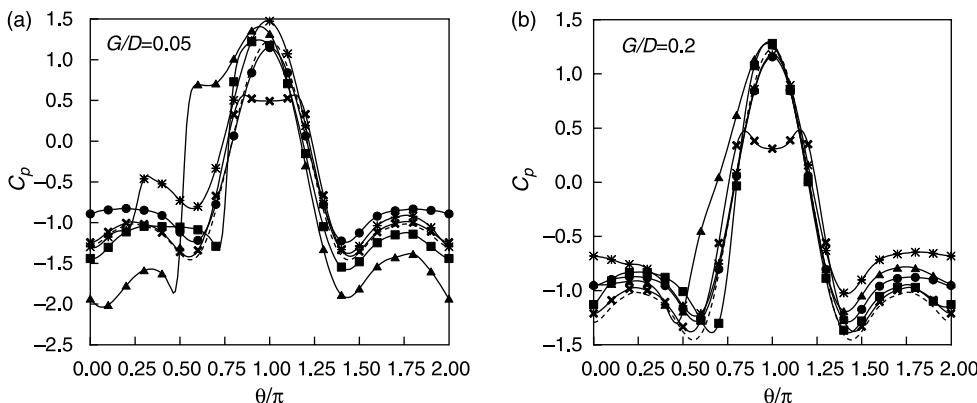
Fig. 11. Time averaged pressure distribution along the perimeter of large cylinder, —●— $\alpha = 0$; —✳—, $\alpha = 0.25\pi$; —+—, $\alpha = 0.5\pi$; —■—, $\alpha = 0.75\pi$; —✕— $\alpha = \pi$; - - -, isolated cylinder for Re$=500$.
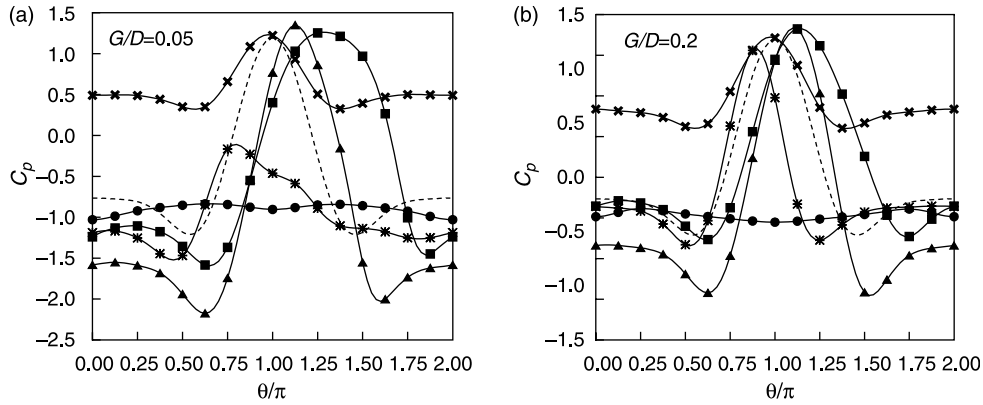
Fig. 12. Time averaged pressure distribution along the perimeter of small cylinder, ●, $\alpha=0$; ✳, $\alpha=0.25\pi$; ⊢, $\alpha=0.5\pi$; ■, $\alpha=0.75\pi$; ✕ $\alpha=\pi$; - - -, isolated cylinder for Re$=500$.

lift is very small and is independent of the location of the small cylinder.

4.2. Pressure distribution

Fig. 11 shows the time averaged pressure coefficient along the perimeter of the large cylinder with the small cylinder located at different positions at two typical gap ratios investigated. For the purpose of the comparison, distribution of time averaged pressure coefficient along an isolated circular cylinder at the same Reynolds number as the one based on the large cylinder diameter is also included in the figure. The pressure coefficient C_p is defined as

$$C_p = \frac{2(p-p_0)}{\rho U^2} \qquad (5)$$

where p_0 is the pressure at a faraway location upstream the cylinders.

Fig. 11(a) shows the mean pressure coefficient distribution along the perimeter of the large cylinder at $G/D=0.05$. It can be clearly seen from Fig. 11(a) that the existence of the small cylinder affects the mean pressure distribution on the large cylinder. The effect of the small cylinder is significant when it is located at around side-by-side locations ($\alpha=0.25\pi$, 0.5π and 0.75π) but less at other two locations. When the small cylinder is located directly behind the large cylinder ($\alpha=0$), it has little effect on the pressure distribution along the upstream part of the large cylinder. However, the mean pressure along the downstream part of the large cylinder increases. The presence of the small cylinder at the trailing edge of the large cylinder prevents the interaction of the vortices across the centerline of the wake and thus, affects the drag and lift on the large cylinder. When the small cylinder is located directly in front of the large cylinder ($\alpha=\pi$), it has little effect on the pressure distribution along the downstream part of the large cylinder and causes a slight pressure decrease along the upstream of part of the cylinder. When the small cylinder is moved towards upstream side of the large cylinder from the wake side of the cylinder ($\alpha=0$), the mean pressure distribution on the large cylinder becomes asymmetric and the pressure coefficient on the downstream side of the large cylinder decreases. The asymmetry and reduction in the wake pressure reach their extremes at $\alpha=0.5\pi$. It is believed that these are the factors responsible for the large values of drag and lift observed at $G/D=0.05$ and $\alpha=0.5\pi$ in Fig. 8.
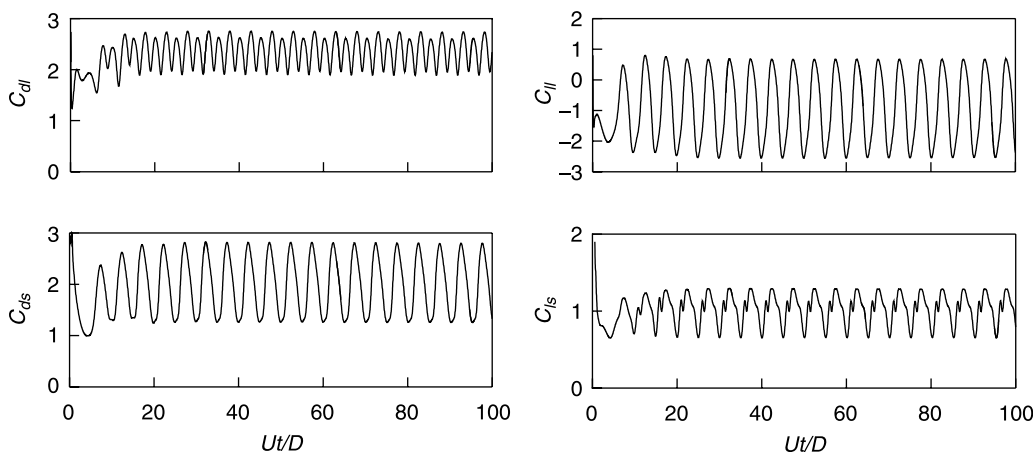
Fig. 13. Time histories of the force coefficients for $G/D=0.05$ and $\alpha=0.5\pi$.

It can be seen from Fig. 11(b) that the effects of the small cylinder on the mean pressure distribution along the large cylinder become weaker as the gap ratio *G/D* increases, although the trends are very similar for the two gap ratios. This indicates that the interaction between the small cylinder and the large cylinder is rather weak at this gap ratio.

Fig. 12 shows the time averaged pressure coefficients along the perimeter of the small cylinder. It can be seen that the pressure distribution on the small cylinder is strongly affected by the location of the small cylinder and relatively less dependent on the gap ratio. This is mainly because that the approaching flow conditions for the small cylinder are very different as it is located at different relative positions to the large cylinder. For example, at $\alpha=0$, the pressure coefficient on the small cylinder is almost a negative constant because

the whole cylinder is immersed in the wake of the large cylinder where the pressure is very small. It is also seen that the pressure distributions are symmetric when the small cylinder is located on the symmetric line at $\alpha=0$ and $\alpha=\pi$. For other cases, the pressure distribution is no symmetric. The stagnation point on the small cylinder shifts to the upper side of the cylinder for $\alpha=\pi/4$, and to the lower side of the cylinder for $\alpha=3\pi/4$ and $\pi/2$. This is the reason for the negative mean lift at $\alpha=\pi/4$ and a positive one at $\alpha=3\pi/4$ and $\pi/2$ as shown in Fig. 9(b).

4.3. Characteristics of vortex shedding from the two cylinders

It has been demonstrated in the Sections 4.1 and 4.2 that the presence of the small cylinder in the vicinity of the large
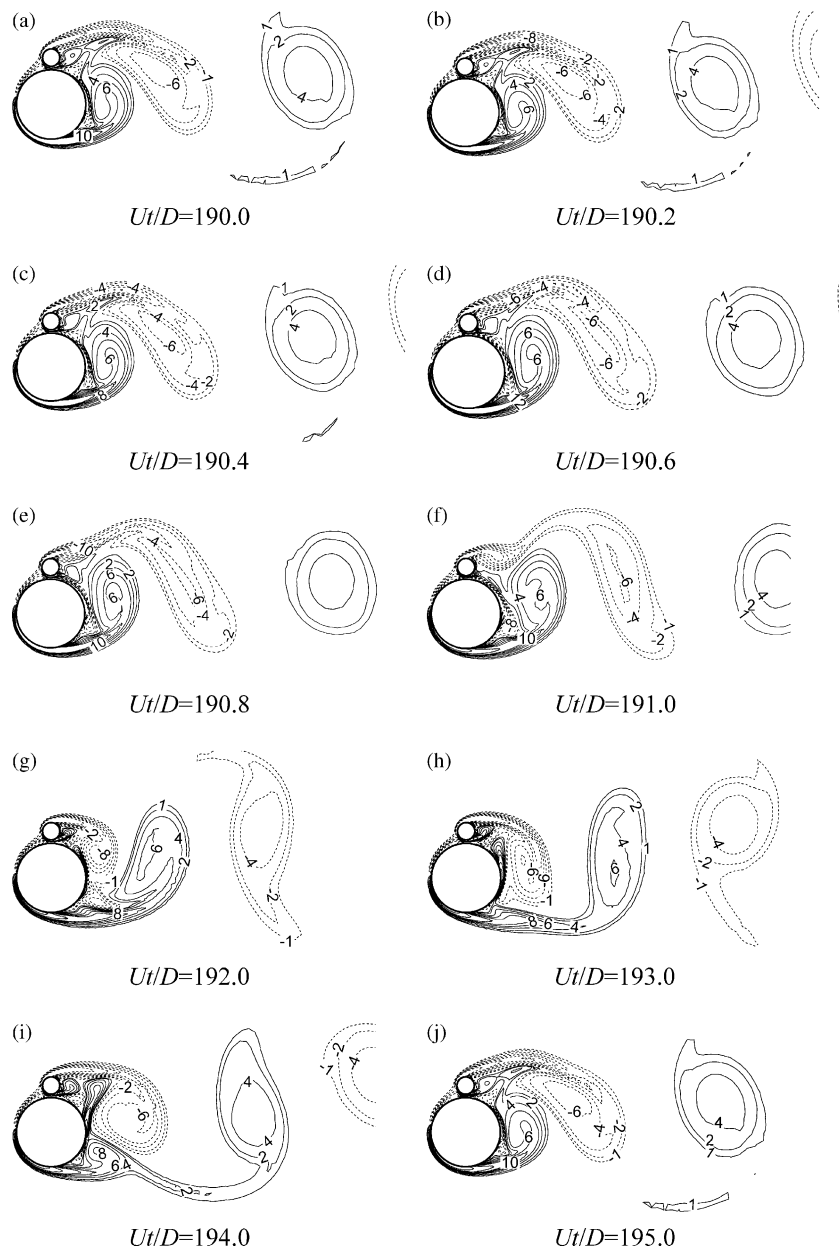
Fig. 14. Instantaneous vorticity contours behind the two cylinders for $G/D=0.05$ and $\alpha=\pi/2$.
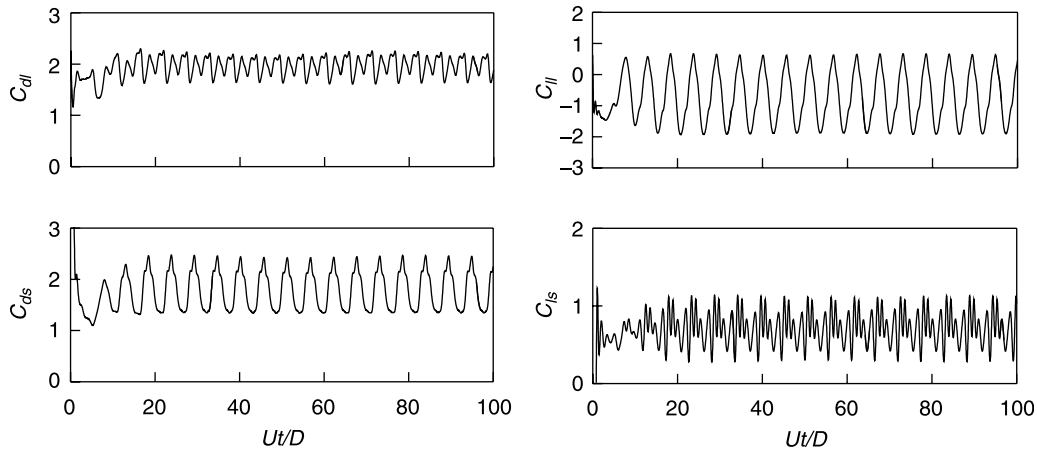
Fig. 15. Time history of the force coefficients for $G/D = 0.1$ and $\alpha = 0.5\pi$.

cylinder induces significant variations of the mean drag, mean lift and the mean pressure distribution on the large cylinder. It is believed that these variations are the direct results of the interactions of vortex shedding from both cylinders. Therefore, the understanding of the vortex shedding characteristics from the two cylinders is of fundamental interests to both practitioners and scientists.

4.3.1. Shedding modes

It is expected that shedding of vortices from the cylinders has different modes, depending mainly on the gap between the two cylinders (G/D). Generally speaking, there will be two shedding processes from the small and large cylinders separately and the interactions between the shedding processes will be weak when the gap between the two cylinders is large. The shedding frequency from the small cylinder will be roughly about four times of that from the large cylinder as the diameter of the large cylinder is four times of that of the small cylinder. When the gap ratio is small enough, it is possible that two separate shedding processes will merge and the two cylinders behave as a single object as far as shedding from them is concerned. Strong shedding interactions are expected at intermediate gap ratios.

Although the level of the interactions between the two shedding processes may be dependent on the angular location of the small cylinder, it is found that the above-mentioned shedding modes exist for the position angle of the smaller cylinder α form 0.125π and 0.875π. Therefore, the numerical results for $\alpha = \pi/2$ will be used to facilitate the discussions in this section.

Fig. 13 shows the time history of the force coefficients on the large and small cylinders for the case of $G/D = 0.05$ and $\alpha = 0.5\pi$, where C_{dl} and C_{ll} are the drag and lift coefficients on the large cylinder and C_{ds} and C_{ls} are the drag and lift coefficients on the small cylinder correspondingly. It can be seen from Fig. 13 that both drag and lift coefficients on the large and small cylinders oscillate at regular frequencies where the frequencies of the drag are about two times of those of the lift correspondingly. This is one of the typical

characteristics of the vortex shedding from an isolated circular cylinder. The frequencies of the drag and lift on both cylinders are approximately equal to the shedding frequency from a single cylinder of an equivalent diameter ($D + d + G$). This suggests that the flow around the two cylinders is similar to the flow around a single cylinder when the gap ratio is 0.05 and $\alpha = 0.5\pi$. Fig. 14 shows instantaneous vorticity contours behind the two cylinders from dimensionless time $Ut/D = 190–195$ for the same case. Regular vortex shedding behind the two cylinders can be clearly observed from Fig. 14. It is seen that the gap plays little role in the shedding process. The strength of the shear layer from the lower edge of the small cylinder is very weak and is dominated by the shedding from the outer sides of the two cylinders. This is consistent with what was observed from the time histories of the drag and lift in Fig. 13. The vortex shedding behavior from the small cylinder can be examined by the small time increment during $Ut/D = 190$ and $Ut/D = 191$ in Fig. 14. Regular vortex shedding from the small cylinder would have been observed at the smaller time interval if it existed. It can be seen from Fig. 14 that there are no shedding of vortices from the lower edge of the small cylinder and the upper tip of the large cylinder. It is quite obvious that the vortices shed from the bottom edge of the large cylinder interact with those shed from the top edge of the small cylinder, forming a single row of wake. There is only one wake from the two cylinders. It is referred to as single-wake shedding mode.

Fig. 15 shows the time history of the force coefficients on the large and small cylinders for the case of $G/D = 0.1$ and $\alpha = 0.5\pi$. The drag and lift coefficients on the large cylinder oscillate in a similar way to those obtained as in the case of $G/D = 0.05$. An interesting phenomenon is found at this gap ratio ($G/D = 0.1$). The drag coefficient on the small cylinder oscillates at a low frequency while the lift coefficient oscillates at a much higher frequency. The time history of the lift coefficient at this gap ratio ($G/D = 0.1$) on the small cylinder is of the typical characteristics of a superposed process of the different frequencies. For this particular case, it seems that

(a) Ut/D=190.0   (b) Ut/D=190.2

(c) Ut/D=190.4   (d) Ut/D=190.6

(e) Ut/D=190.8   (f) Ut/D=191.0

(g) Ut/D=192.0   (h) Ut/D=193.0

(i) Ut/D=194.0   (j) Ut/D=195.0
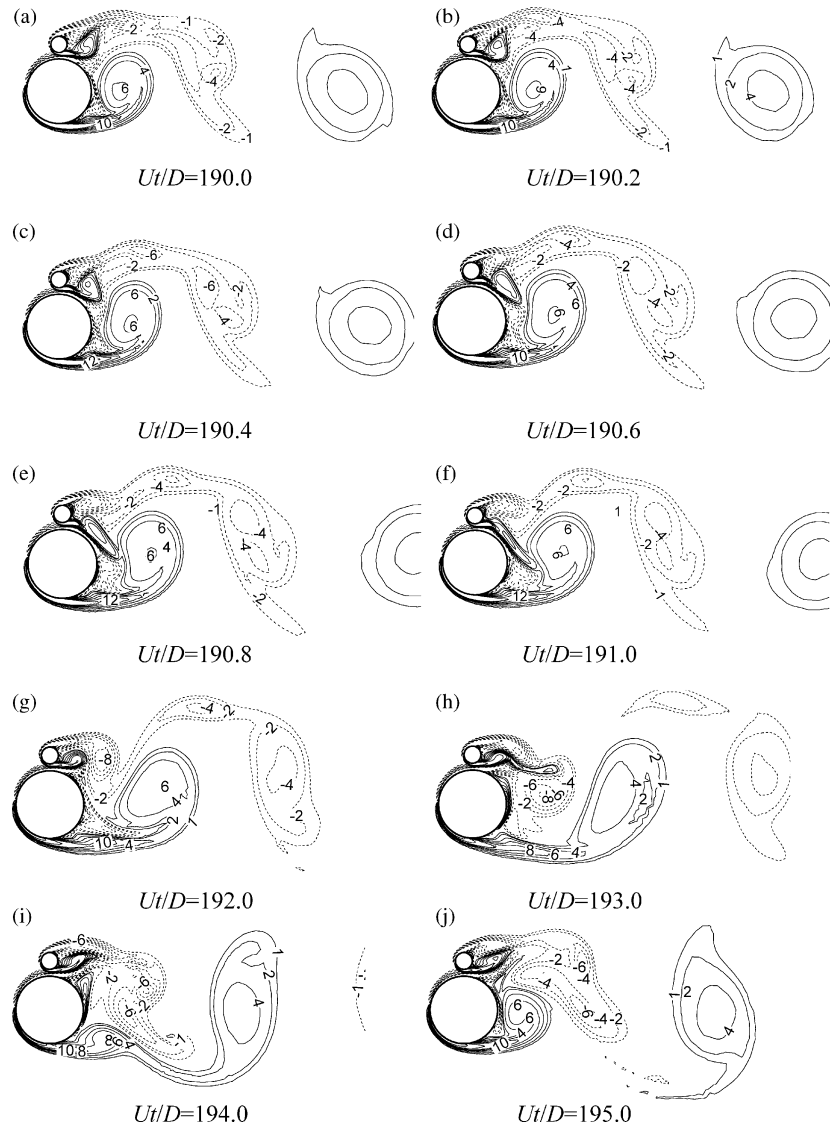
Fig. 16. Instantaneous vorticity contours behind the two cylinders for G/D=0.1 and $\alpha = \pi/2$.
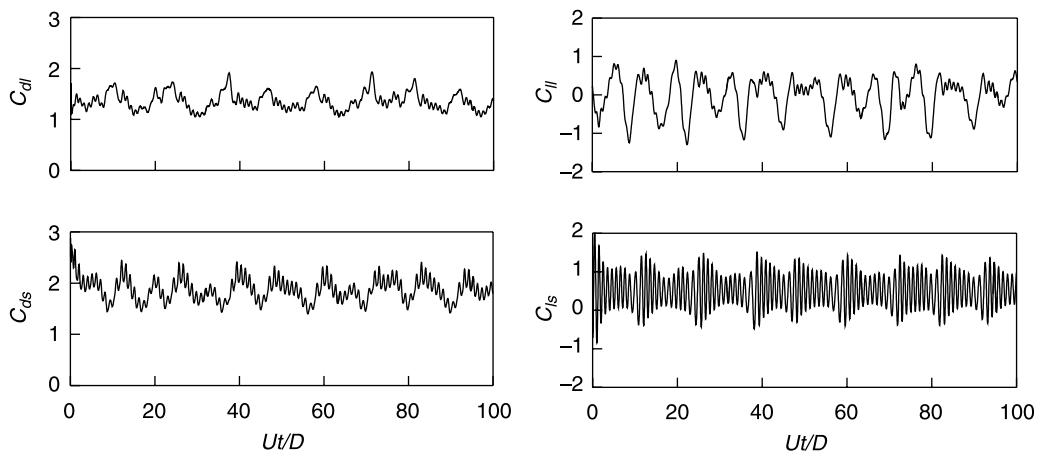
Fig. 17. Time history of the force coefficients for G/D=0.3 and $\alpha = 0.5\pi$.
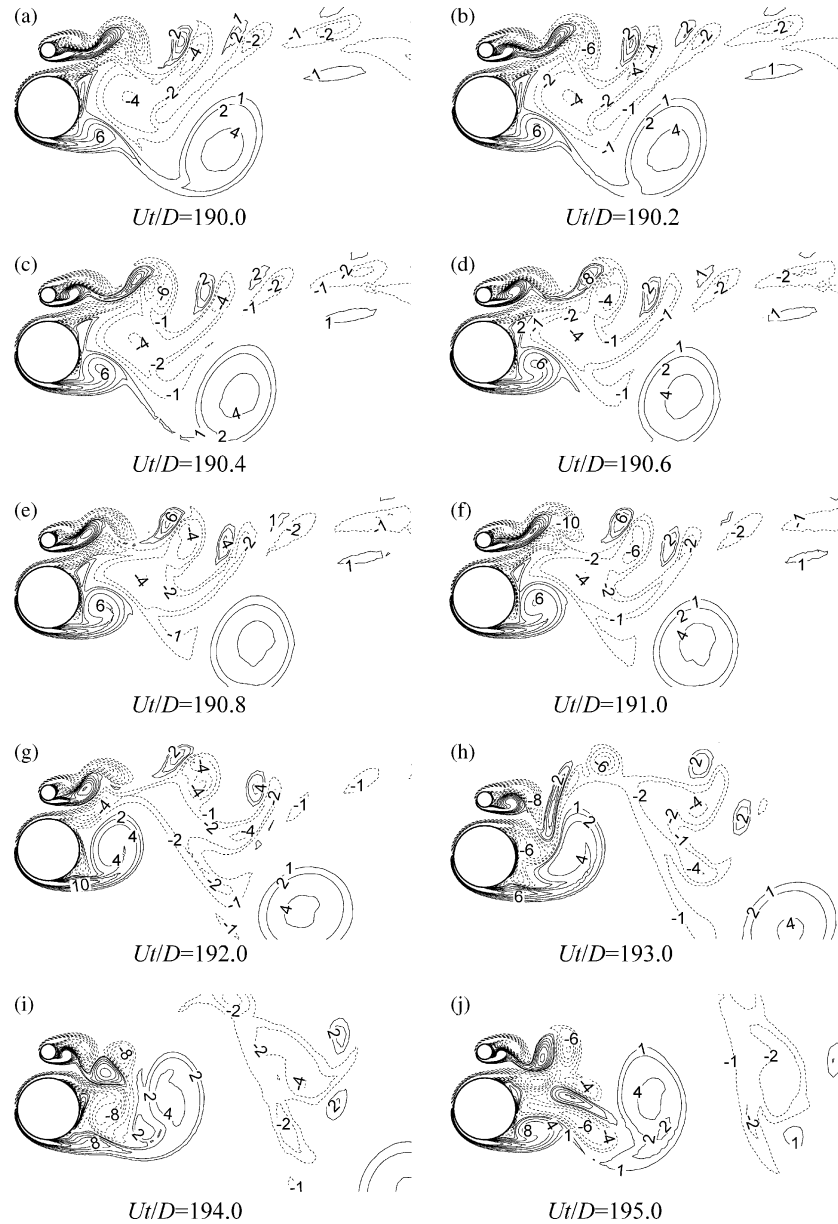
Fig. 18. Instantaneous vorticity contours behind the two cylinders for $G/D=0.3$ and $\alpha=\pi/2$.

the low frequency component predominates. It can be clearly seen that the high frequency component is superposed on the low frequency component. The low frequency component seems to have a frequency close to the frequency of vortex shedding from a circular cylinder of an equivalent diameter. The high frequency component has a frequency corresponding to the frequency of vortex shedding from a circular cylinder of a diameter around that of the small cylinder. It is likely that shedding from the small cylinder co-exists with the single-wake shedding mode at this gap ratio but the shedding from the small cylinder is rather weak. Fig. 16 shows instantaneous vorticity contours behind the two cylinders for roughly one vortex shedding period. In addition to the regular vortex shedding behind the two cylinders as seen for the case of $G/D=0.05$, the changes in the wake structure behind the small cylinder are more obvious than the case with

$G/D=0.05$. The non-dimensional period of the regular vortex shedding from the small cylinder would be around one if it does exist. It can be seen from Fig. 16((a)–(f)) that although no obvious regular shedding of vortices from the small cylinder exists, a vortex is shed regularly from the gap between two cylinders at a non-dimensional period of around 1.0. It is believed that the shedding of the vortices from the gap is due to the interactions of the shear layers from the bottom edge of the small cylinder and the top edge of the large cylinder and is responsible for the high frequency lift on the small cylinder as shown in Fig. 15. It is not difficult to see that the vortex shedding is transiting from the single-wake mode to the two shedding mode at this gap ratio ($G/D=0.1$).

Fig. 17 shows the time history of the force coefficients on the large and small cylinders for the case of $G/D=0.3$ and $\alpha=0.5\pi$. It can be seen from Fig. 17 that although the drag
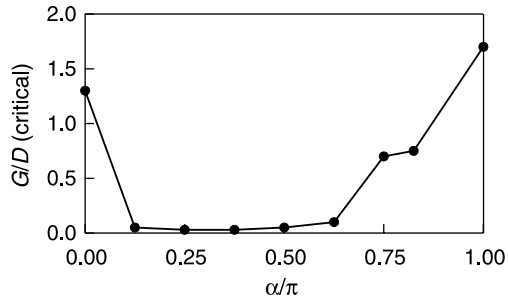
Fig. 19. Critical gap ratio below which the single-wake shedding mode exists.

and lift coefficients on the large cylinder still oscillate mainly at the low frequency, there are clearly high frequency components superposed on the low frequency drag and lift. It is obvious that the low frequency corresponds to the frequency of the vortex shedding from the large cylinder and the high frequency corresponds to the shedding frequency from the small cylinder. This becomes more obvious if the drag and lift on the small cylinder are examined (Fig. 17). The lift on the small cylinder clearly oscillates at a frequency corresponding to the shedding frequency from the small cylinder and the high frequency component on the drag becomes stronger. This suggests that there exist two vortex shedding processes behind the two cylinders, i.e. one from the large cylinder and the other from the small cylinder. This is further confirmed by examining the vorticity contours behind the cylinders as shown in Fig. 18. It is clearly seen in Fig. 18 that two shedding processes exist behind the two cylinders and the two shedding processes interact with each other. This mode is referred to as interaction shedding mode.

As the gap ratio further increases, it is observed from the numerical results that the interactions between the two shedding processes become weaker and the shedding behind the two cylinders become relatively independent. This is called the two-wake mode. Due to the page limit of the paper, these figures are not presented here.

The three vortex shedding modes discussed above exist for the position angle of the smaller cylinder α form 0.125π and 0.875π. If the two cylinders are in near tandem arrangement, the flow pattern around the downstream cylinder is affected by the shedding from the upstream cylinder for the gap G/D investigated in this study. However, the single-wake mode exits for small gaps regardless of angular location of the small cylinder. The critical gap ratio below which the shedding is in the single-wake shedding mode is dependent on the angular location of the small cylinder. Fig.19 shows the critical ratio for different angular locations of the small cylinder. It can be seen that the critical gap ratio is very small and almost a constant for $0.125\pi < \alpha < 0.625\pi$. The critical gap ratio increases sharply when the angular location is outside this range.

4.3.2. Power spectra of the fluctuating lift force

Fourier analyses of the lift coefficients on the cylinders are carried out for all the gap ratios and angular locations. Fig. 20 shows the power spectra of the fluctuating lift on the large cylinder for $\alpha=0.5\pi$ and different values of G/D. The spectra of the lift on the large cylinder have one dominant sharp peak frequency for large and small values of gap ratio G/D. For small values of G/D, since there is only one wake behind the cylinders, the power spectra have only one peak frequency. This confirms the single-wake shedding mode at small gap ratios. For large values of G/D, since there are two shedding processes behind the two cylinders and the interaction between the shedding from the large cylinder and the shedding from the small cylinder is weak, the lift is dominated by the shedding
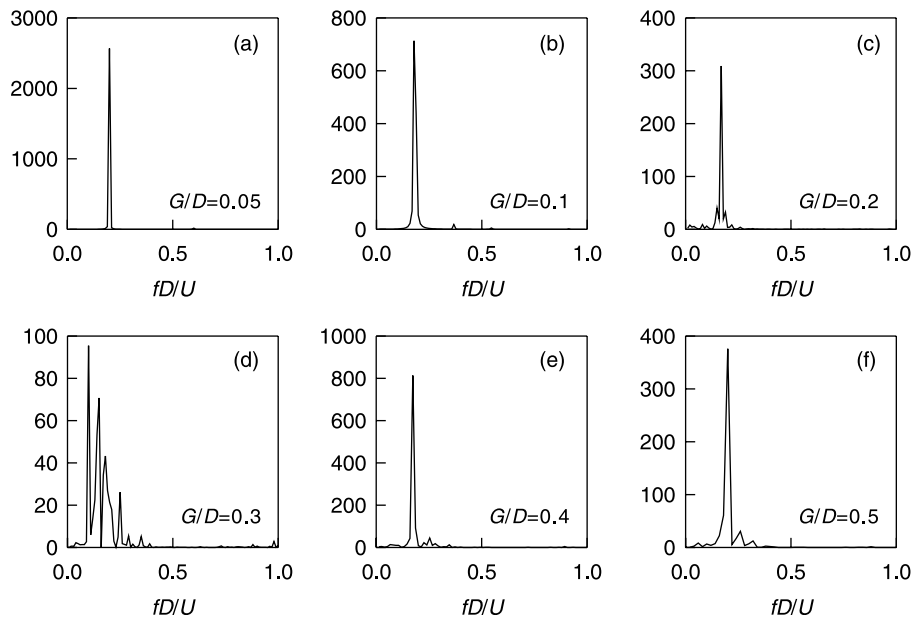
Fig. 20. Power spectra of the lift forces on the large cylinder for $\alpha=0.5\pi$ and different values of G/D.
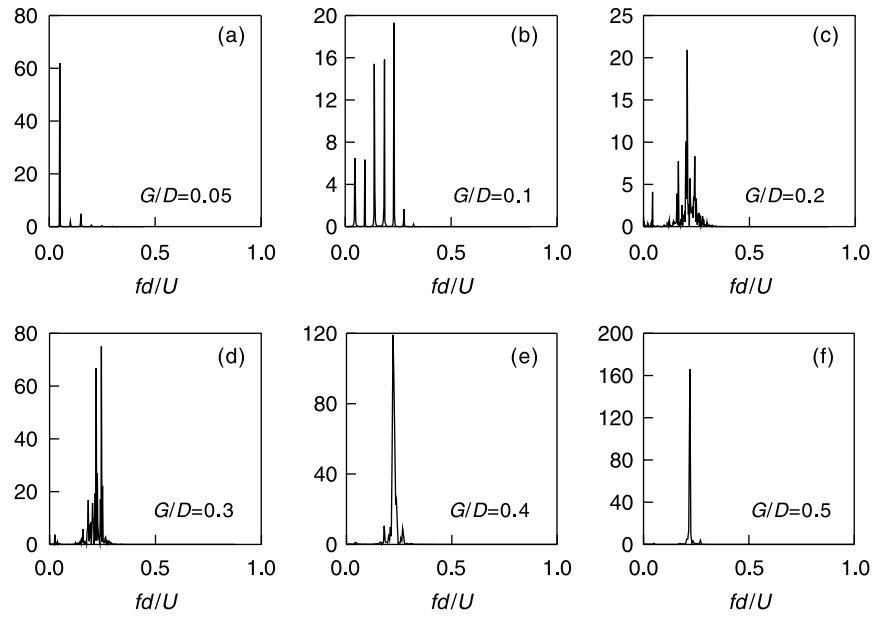
Fig. 21. Power spectrum of the lift forces on the small cylinder for $\alpha = 0.5\pi$ and different *G/D*.

from the large cylinder and only one dominant sharp peak is detected in the power spectrum. For the medium gap ratios the spectra are broad banded because of the interaction of the wakes behind the two cylinders.

Fig. 21 shows the power spectra of the lift on the small cylinder for $\alpha = 0.5\pi$ and different values of *G/D*. It is seen that for *G/D*=0.1, the power spectra has multiple peak frequencies and the power at these peak frequencies is of similar order of magnitudes. This confirms the previous finding that the vortex shedding is in the transitional mode at this gap ratio. As the gap

ratio increases to *G/D*=0.2 and 0.3, the multiple peak frequency is still a dominant feature of the power spectra. This indicates strong interactions between the two shedding processes. The fundamental frequency becomes more dominant as the gap ratio further increases. This indicates the interaction between the two shedding processes become weaker as the gap ratio becomes larger.

Fig. 22 shows the power spectra of the total lift on two cylinders for $\alpha = 0.5\pi$ and different values of *G/D*. The normalized frequency is based on the large cylinder diameter
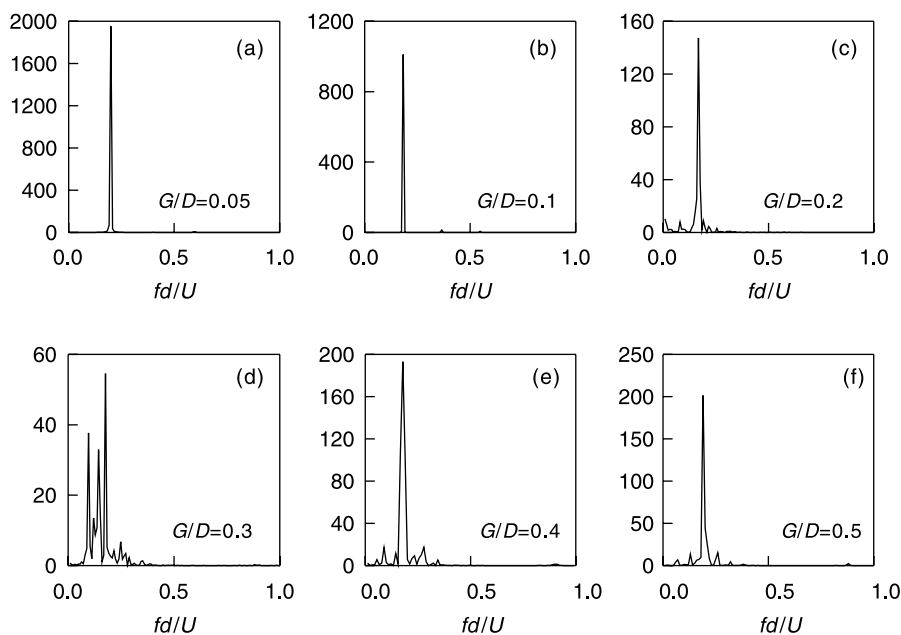
Fig. 22. Power spectrum of the total lift forces for $\alpha = 0.5\pi$ and different *G/D*.
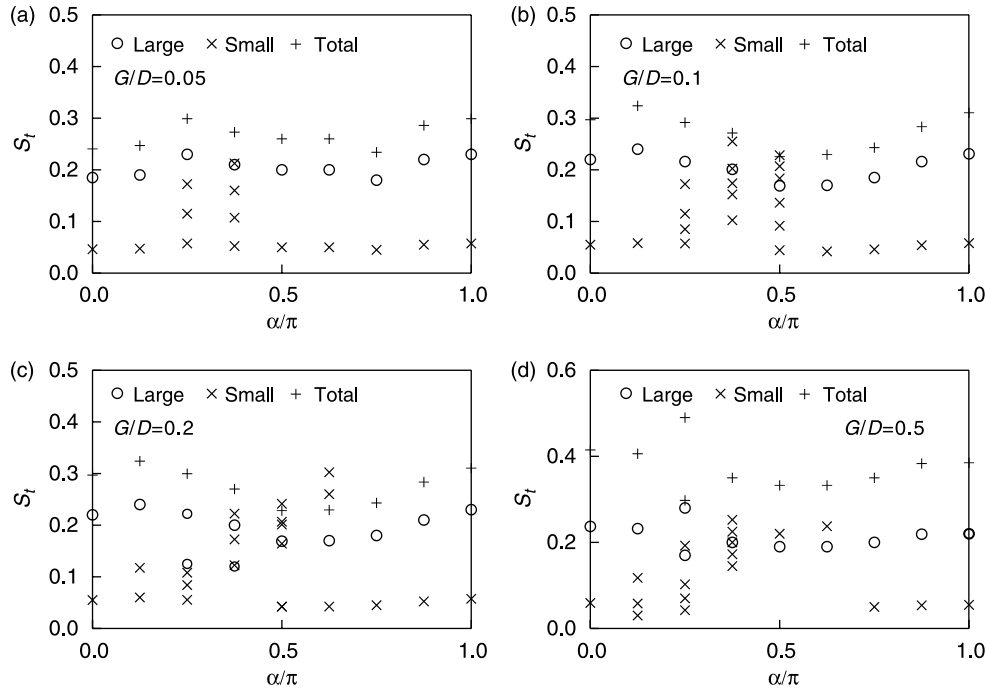
Fig. 23. Strouhal number.

for the purpose of comparison. It can be seen that the power spectra of the total lift are very similar to those of the large cylinder. This is because the force on the large cylinder dominates the total force.

4.3.3. Shedding frequency

The Strouhal number of the lift force on the cylinders is studied. The definitions of the Strouhal number for the small, large and the equivalent cylinders are based on their independent diameters.

Fig. 23 shows the Strouhal numbers of the lift coefficients for $G/D=0.05$, 0.1, 0.2 and 0.5. For $G/D=0.05$ and 0.1, it is found that the lift force on the large cylinder and total lift force almost fluctuate at the same dimensional frequency. This is because the shedding frequency of the total lift is completely dominated by the frequency of the lift on the large cylinder, regardless of the angular location and the gap ratio. For $G/D=0.05$ and 0.1, it is observed that the power spectra of the lift force on the small cylinder have several sharp peak frequencies as the position angle α is around 0.25π to 0.5π (as shown in Fig. 21(b) and (c)). In these cases, all values of the Strouhal number based on the sharp peak frequencies are plotted in Fig. 23. For $G/D=0.2$ and 0.5, the power spectra of the lift force on both of the large cylinder and the small cylinder are either multi-peak or broad-banded (Figs. 20(c) and 21(d)). For the broad-banded spectra, several maximum peak frequencies are plotted in Fig. 23. The interaction of the vortexes becomes drastic for these gap ratios as discussed in Section 4.3.1.

The dimensional frequency of the lift on the small cylinder is the same as those of the large cylinder (the Strouhal number of the small cylinder is one-fourth of that of the large cylinder) for the large and small values of the position angle of the small

cylinder. It is quite obvious that the two cylinders act as a single body for small gap ratios and as independent bodies as for large gap ratios.

Fig. 24 shows the Strouhal number normalized using the values of the Strouhal number corresponding to a single cylinder. For the lift with multi-peak frequencies or broad-banded spectra, the Strouhal number in Fig. 24 is based on the frequency corresponding to the maximum power. It can be seen from Fig. 24 that the frequency for the large cylinder is generally smaller than that of a single cylinder at the same Reynolds number. The frequency for the small cylinder is larger than that of a single cylinder except for $G/D=0.05$. For $G/D=0.05$, the lift on the small cylinder fluctuates in the same frequency as that of the large cylinder. For G/D ranging from 0.05 to 0.5, the Reynolds number based on the equivalent cylinder diameter is 650 to 875, and the computed Strouhal number for an isolated cylinder by those Reynolds number ranges from 0.233 to 0.236. These values are close to a value of 0.227, which is
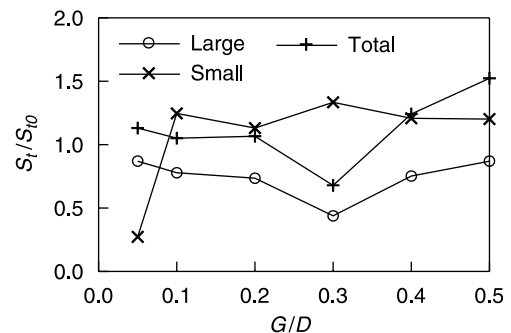
Fig. 24. Normalized Strouhal number, $G/D=0.05$; , $G/D=0.1$; , $G/D=0.2$; , $G/D=0.5$; , $G/D=1.0$; , $G/D=\infty$.
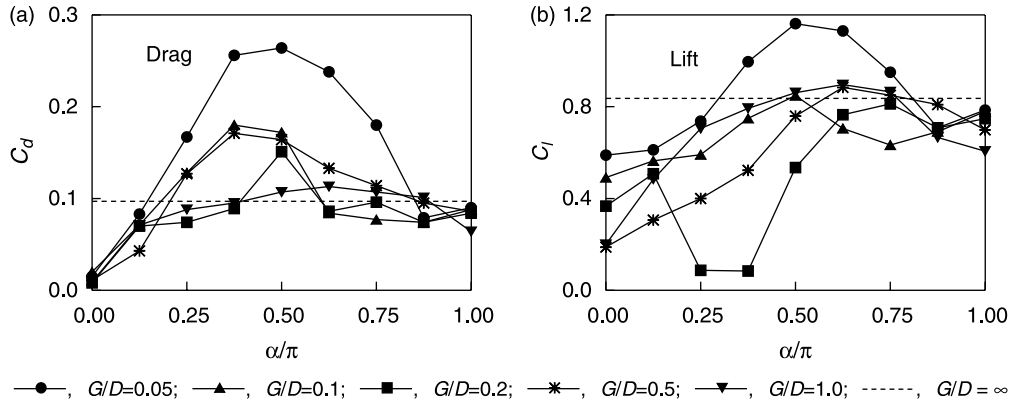
Fig. 25. RMS of the force coefficients on the large cylinder, —●— G/D=0.05; ←, G/D=0.1; —■—, G/D=0.2; —✳—, G/D=0.5; —▼—, G/D=1.0; - - -, G/D=∞.

the Strouhal number of a single cylinder for Re=500. So, the normalized Strouhal number of the total lift is about D_e/D times that of the large cylinder. The minimum Strouhal number of the lift on the large cylinder and the total lift occurs at G/D=0.3. This indicates the strongest interaction between the large and small cylinders. The influence of the small cylinder is strongest at G/D=0.3. It can be seen that the actual Strouhal number of the total lift is greater than that on the equivalent cylinder except for G/D=0.3 in the computed ranges of G/D.

4.3.4. Root-Mean-Square (RMS) forces

The RMS force coefficients on the cylinders are studied. Fig. 25 shows the RMS force coefficients on the large cylinder. The RMS force coefficients on an isolated cylinder at the same Reynolds number is also plotted in Fig. 25 for the purpose of comparison. The RMS drag coefficient is smaller than that of a single cylinder as the small cylinder is located in front of or behind the large cylinder, and larger as the small cylinder is at the side of the large cylinder. At a very small value of G/D, the RMS lift on the large cylinder is larger than that on an isolated cylinder if the small cylinder is located at the side of

the large cylinder. The RMS lift on the large cylinder is smaller than that on an isolated cylinder, at larger values of G/D.

Fig. 26 shows the RMS force coefficients on the small cylinder. The RMS drag coefficients on the small cylinder are much larger than that on an isolated cylinder at the same Reynolds number except for $\alpha=\pi$. It is seen that the RMS lift on the small cylinder for $\alpha=\pi$ is much smaller than that for $\alpha=0$. For $\alpha=0$, the smaller cylinder is immersed in the wake of the large cylinder. The vortices shed from the upper and the lower edges of the large cylinder induce a large value of lift on the small cylinder. For $\alpha=\pi$, there would not be vortices shed from the small cylinder at small value of G/D. The vortices shed behind the small cylinder may be weaker than those shed from behind of the large cylinder at larger values of G/D. So, the lift for $\alpha=\pi$ on the small cylinder is much smaller than that for $\alpha=0$.

Fig. 27 shows the RMS of the total force coefficient on two cylinders. The total force coefficients on two cylinders are based on the equivalent cylinder diameter ($D_e=D+d+G$). Because the force component of the large cylinder is dominative in the total force coefficient, the variation of the total RMS force coefficient is very similar to that on the large cylinder. For larger value of G/D, both the RMS drag
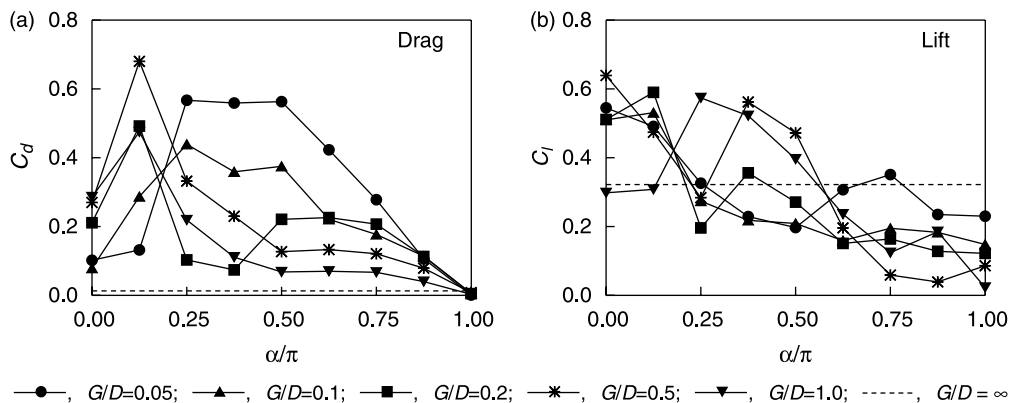
Fig. 26. RMS of the force coefficients on the small cylinder, —●— G/D=0.05; ←, G/D=0.1; —■—, G/D=0.2; —✳—, G/D=0.5; —▼—, G/D=1.0; - - -, G/D=∞.
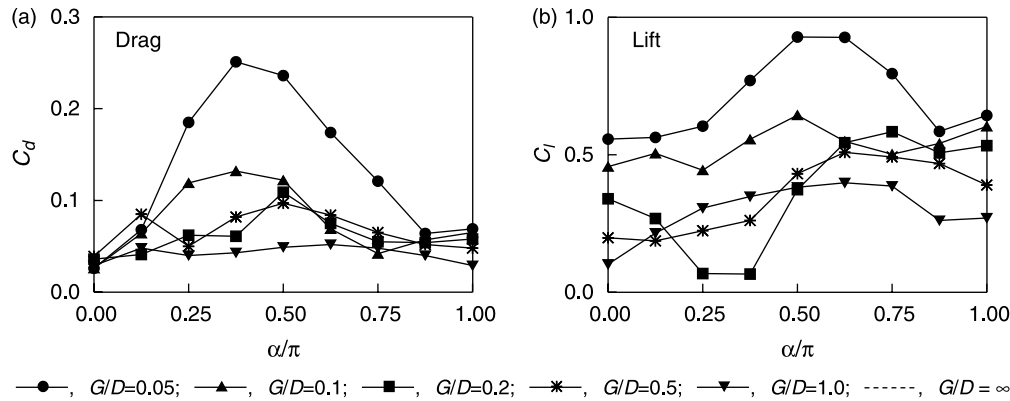
Fig. 27. RMS of the force coefficients on the two-cylinder system, —●—, $G/D=0.05$; ◂-, $G/D=0.1$; —■—, $G/D=0.2$; —✳— $G/D=0.5$; —▼—, $G/D=1.0$; - - -, $G/D=\infty$.

and lift coefficients become smaller because the equivalent cylinder diameter becomes larger.

5. Conclusions

In this study, vortex shedding from two cylinders of different diameters is studied numerically. The two-dimensional Navier-Stokes equations are solved by using a finite element method. The flow is calculated for a broad range of gap ratios and angular locations of the small cylinder. The effects of the gap ratio and the angular location of the small cylinder on the vortex shedding are investigated. The major results can be summarized as follows:

1. For the position angle of the smaller cylinder α form 0.125π and 0.875π, the shedding flow behind the two cylinders can be classified into three types. For the very small gap ratio, there is only one wake behind the two cylinders. It is referred to as single-wake shedding mode. At medium gap ratios, there exist strong interactions between the vortex shedding from the large cylinder and the shedding from the small cylinder. This is called interaction mode. For very large gap ratios, the interaction between the shedding from the two cylinders becomes very weak. This is called two-wake mode. If the two cylinders are in near tandem arrangement, the flow pattern around the downstream cylinder is always affected by the shedding from the upstream cylinder for the gap G/D investigated in this study, but the single-wake shedding mode does exist in case of small G/D.

2. The time-averaged mean drag forces on the large and the small cylinders attain the maximum values as α is around $\pi/2$. The mean drag force on the large cylinder increases with increase of gap ratio as α is around $\pi/2$. However, the gap ratio does not affect the drag on the small cylinder very much. For a given gap ratio, the mean lift on the large cylinder attains its maximum value as $\alpha=\pi/2$, whereas the maximum mean lift force on the small cylinder is found at $\alpha=3\pi/4$.

3. The total mean drag on the two cylinders is generally smaller than its counterpart on an equivalent cylinder for most of the gap ratios and angular locations of the small cylinder except for very small gap ratios, i.e. $G/D=0.05$ and $G/D=0.1$, where total mean drag on the two cylinders is greater than that on the equivalent cylinder for roughly $0.25\pi<\alpha<0.5\pi$. The smaller the gap ratio, the larger total mean drag is. At the minimum gap ratio examined ($G/D=0.05$), the total mean drag could be 1.5 times as large as that on the equivalent cylinder when $\alpha=0.5\pi$. For $\alpha=0.5\pi$, the total mean lift force on the two cylinders is non-zero for smaller gap ratios $G/D=0.05$ and 0.1. The total mean lift could be downward or upward depending on the location of the small cylinder. For $G/D=0.2$, 0.4 and 1.0, the total mean lift is very small.

4. Vortex shedding frequency for the large cylinder is generally smaller than that of a single cylinder at the same Reynolds number. The frequency for the small cylinder is larger than that of a single cylinder except for $G/D=0.05$. For $G/D=0.05$, the lift force on the small cylinder fluctuates in the same frequency as that of the large cylinder. The minimum Strouhal number of the lift on the large cylinder occurs at $G/D=0.3$. The Strouhal number of the total fluctuating lift is always smaller than that on the equivalent cylinder.

5. The RMS force coefficients on the large cylinder, the small cylinder and the RMS of total force coefficients are strongly affected by the location of the small cylinder and the gap ratio. The RMS forces coefficients generally increase as the gap ratio decreases and the small cylinder approaches to the side-by-side location.

6. Since, the present study is carried out at a rather small Reynolds number, the findings reported in this study need to be verified before they can be employed in pipeline designs.

7. It is recognized that the diameter ratio of the large and small cylinders will also affect the hydrodynamic forces on the cylinders and vortex shedding behavior from the two cylinders and this will be investigated in a future study.

Acknowledgements

References

[1] Zdravkovich MM. Review of flow interference between two circular cylinders in various arrangements. ASME, J Fluids Eng 1977;99: 618–33.

[2] Zdravkovich MM. The effects of interference between circular cylinders in cross flow. J Fluids and Struct 1987;1:239–61.

[3] Bearman PW, Wadcock AJ. The interaction between a pair of circular cylinder normal to a stream. J Fluid Mech 1973;61:499–511.

[4] Williamson CHK. Evolution of a single wake behind a pair of bluff bodies. J Fluid Mech 1985;159:1–18.

[5] Kim HJ, Durbin PA. Investigation of the flow between a pair of cylinders in the flopping regime. J Fluid Mech 1988;196:431–48.

[6] Meneghini JR, Saltara F, Siqueira CLR, Ferrari Jr. JA. Numerical simulation of flow interference between two circular cylinders in tandem and side-by-side arrangements. J Fluids and Struct 2001;15:327–50.

[7] Mittal S, Kumar V, Raghuvanshi A. Unsteady incompressible flows past two cylinders in tandem and staggered arrangements. Int J Numer Methods Fluids 1997;15:1315–44.

[8] Strykowski BJ, Sreenivasan KR. On the formation and suppression of vortex 'shedding' at low Reynolds numbers. J Fluid Mech 1990;218: 71–107.

[9] Sakamoto H, Tan K, Haniu H. An optimum suppression of fluid forces by controlling a shear layer separated from a square prism. J Fluids Eng 1991;113:183–9.

[10] Sakamoto H, Haniu H. Optimum suppression of fluid forces acting on a circular cylinder. J Fluids Eng 1994;116:221–7.

[11] Dalton C, Xu Y, Owen JC. The Suppression of lift on a circular cylinder due to vortex shedding at moderate Reynolds numbers. J Fluids Struct 2001;15:617–28.

[12] Williamson CHK. The existence of two stages in the transition to three dimensionality of a cylinder wake. Phys Fluids 1988;31(11): 3165–8.

[13] Williamson CHK. Oblique and parallel modes of vortex shedding in the wake of a circular cylinder at low Reynolds numbers. J Fluid Mech 1989; 26:576–626.

[14] Jiang CB, Kawahara M. The analysis of unsteady incompressible flows by a three-step finite element method. Inter J Numer Methods Fluids 1993; 16:793–811.

[15] Lei C, Cheng L, Armfield SW, Kavanagh K. Vortex shedding suppression for flow over a circular cylinder near a plane boundary. Ocean Eng 2000; 27:1109–27.

[16] Jester W, Kallinderis Y. Numerical study of incompressible flow about fixed cylinder pairs. J Fluids and Struct 2003;17:561–77.

[17] Braza M, Chassaing P, Ha Minh H. Numerical study and physical analysis of the pressure and velocity fields in the near wake of a circular cylinder. J Fluid Mech 1986;165:79–130.

[18] Tritton DJ. Experiments on the flow past a circular cylinder at low Reynolds numbers. J Fluid Mech 1959;6:547–67.

[19] Lei C, Cheng L, Kavanagh K. A finite difference solution of the shear flow over a circular cylinder. Ocean Eng 2000;27:271–90.

[20] Roshko A. Technical Note 2913, National Advisory Committee for Aeronautics (NACA), Washington; 1953.